NANO LETTERS

pubs.acs.org/NanoLett Letter

Directed Exciton Magnetic Polaron Formation in a Single Colloidal Mn^{2+}:CdSe/CdS Quantum Dot

Severin Lorenz, Christian S. Erickson, Maurizio Riesner, Daniel R. Gamelin, Rachel Fainblat,* and Gerd Bacher

Cite This: *Nano Lett.* 2020, 20, 1896−1906 Read Online

ACCESS | Metrics & More | Article Recommendations | Supporting Information

ABSTRACT: One of the most prominent signatures of transition-metal doping in colloidal nanocrystals is the formation of charge carrier-induced magnetization of the dopant spin sublattice, called exciton magnetic polaron (EMP). Understanding the direction of EMP formation, however, is still a major obstacle. Here, we present a series of temperature-dependent photoluminescence studies on single colloidal Mn^{2+}:CdSe/CdS core/shell quantum dots (QDs) performed in a vector magnetic field providing a unique insight into the interaction between individual excitons and numerous magnetic impurities. The energy of the QD emission and its full width at half-maximum are controlled by the interplay of EMP formation and statistical magnetic fluctuations, in excellent agreement with theory. Most important, we give the first direct demonstration that anisotropy effects—hypothesized for more than a decade—dominate the direction of EMP formation. Our findings reveal a pathway for directing the orientation of optically induced magnetization in colloidal nanocrystals.

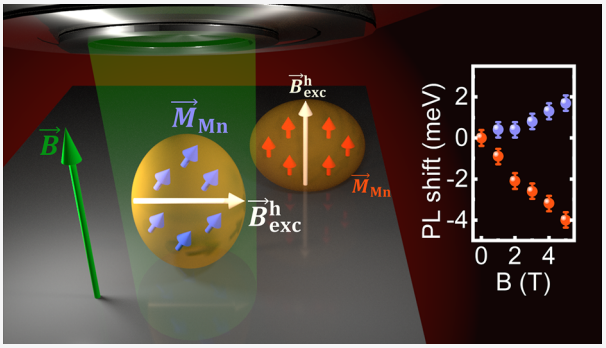

KEYWORDS: *Single nanocrystal, transition-metal doping, exciton magnetic polaron, magnetization fluctuation, quantum dot anisotropy, vector magnetic field*

Recent advances in chemical synthesis enable the design of tailored, high-quality nanocrystals with small size dispersions, a wide variety of shapes, and complex geometries.[1,2] One of the most enduring challenges in this field has been the use of controlled doping, that is, replacing individual atoms in the crystal matrix by impurities, to control the physical properties of such nanocrystals.[3−6] Dopants may act as emission centers, affecting the luminescence of the host material.[7−16] Introducing open-shell transition-metal ions such as cobalt or manganese into nonmagnetic semiconductors endows the host nanocrystals with magnetic functionalities.[17−25] Exchange interactions between the localized magnetic moments of the dopants' *d* electrons and the magnetic moments of the delocalized charge carriers (*s*-type electrons and *p*-type holes) result in giant magneto-optical responses.[26,27] This development was boosted by the prediction of huge exchange fields in colloidal quantum dots (QDs),[28] making room-temperature applications feasible. Indeed, giant Zeeman splittings have been observed up to room temperature in various colloidal nanocrystals.[6,29,30] Among the most intriguing consequences of the pronounced *sp*−*d* exchange interactions is the spontaneous alignment of the dopant magnetic moments mediated by photogenerated charge carriers in the host QDs,[31−34] the so-called exciton magnetic polaron (EMP) formation. In colloidal QDs, these EMPs have been demonstrated to be stable up to room temperature[31] and even accessible by electrical charge carrier injection.[35] Another fundamental consequence of the finite number of magnetic dopants inside a colloidal QD is the occurrence of thermodynamic spin fluctuations, modifying, for example, EMP formation[32] and carrier spin dynamics.[33]

Until now, EMP formation in doped nanocrystals has only been investigated in nanocrystal ensembles,[31−34] where unavoidable inhomogeneous broadening effects cover fundamental physical properties due to distributions of nanocrystal shape, size, composition, and orientation within the ensemble. As an example, anisotropic EMP formation has been theoretically predicted[36,37] and used to explain long relaxation times of optically excited EMPs in Mn^{2+}-doped CdSe QDs,[31,32] but such anisotropy has never been directly observed experimentally.

In a very limited number of cases, experiments on transition-metal-doped colloidal nanocrystals have been extended to single QD studies, mostly focusing on the luminescence of the

Received: December 13, 2019
Revised: January 28, 2020
Published: January 30, 2020

https://dx.doi.org/10.1021/acs.nanolett.9b05136
Nano Lett. 2020, 20, 1896−1906

internal dopant ligand field transition[12,38] and its intermittency.[39−41] In addition, fine structure effects of excitonic luminescence caused by individual Mn^{2+} dopants in single nanocrystals have been addressed.[42] This limited body of experimental literature is quite surprising in two aspects: First, single nanocrystal spectroscopy gave valuable input for the research on undoped semiconductor nanocrystals, for example, by revealing luminescence blinking caused by a statistical redistribution of charge carriers,[43,44] their impact on radiative recombination dynamics,[45] and spectral diffusion,[46] as well as the control of these effects via core/shell architectures.[47] In addition, electric field-induced Stark shifts,[48] fine structure splitting due to $s-p$ exchange,[49] and their tuning in a magnetic field,[50] or multiexciton emission[51,52] have been studied, among others. Second, single QD spectroscopy has been applied to epitaxially grown semiconductors doped with transition metals, demonstrating coupling between excitons and individual dopants[53−56] and revealing EMP formation[57−60] as well as spin fluctuations[57,61−63] in a highly anisotropic system characterized by strong quantum confinement along the growth axis and a rather weak one perpendicular to it.

In this work, we present magneto-photoluminescence (PL) spectroscopy studies of EMP formation in single colloidal Mn^{2+}:CdSe/CdS QDs with wurtzite crystal structure (see Supporting Information). Statistical fluctuations of the Mn^{2+} magnetization are found to be the source of a pronounced broadening of single QD emission line width at low temperatures. A distinct shift in energy with temperature and magnetic field, combined with a characteristic change in full width at half-maximum (FWHM), is observed for a series of individual QDs. The uniquely detailed set of data gained for single QDs is described well by a theoretical model considering the interplay of EMP formation and thermodynamic spin fluctuations. Most interesting, unambiguous signatures of anisotropy effects on both the direction and stability of EMP formation and on statistical fluctuations of the Mn^{2+} spins are found. By applying a three-dimensional (3D) vector magnetic field, we demonstrate that EMP formation can be manipulated, that is, stabilized (increase of EMP binding energy) or destabilized (decrease of EMP binding energy), by varying the angle between the external magnetic field and a dominant anisotropy axis of the nanocrystals. This EMP stabilization and destabilization in addition affect thermodynamic spin fluctuations visualized by a corresponding decrease and increase of the excitonic line width, respectively.

Results and Discussion. Mn^{2+}-doped CdSe/CdS nanocrystals (core diameter: 5.8 nm, total diameter: 11.9 nm) with an average dopant concentration of x_{Mn} = 0.9% were synthesized for single QD experiments by diffusion doping.[6,20,32] Undoped CdSe/CdS QDs with similar core/shell structure were prepared as a reference (see SI for further information). Both samples use giant CdS shells to minimize the overlap of the hole wave function with surface trap states, while attracting the electron via Coulomb interaction close to the core. Surface traps are often reported to induce PL intermittency and spectral diffusion.[46,47,64] Details about sample fabrication for spatially resolved PL experiments can be found in the SI.

Figure 1 depicts the temperature-dependent PL spectra of (a) a single undoped CdSe/CdS QD and (b) a single Mn^{2+}-doped CdSe/CdS QD (QD #1). The PL of the undoped QD exhibits a narrow zero phonon line (ZPL) with a FWHM of 1.1 meV (limited by the spectral resolution of our experimental setup), in agreement with literature values for comparable excitation intensities of ≤10 Wcm^{-2}.[65] A weak phonon replica, related to the simultaneous emission of a longitudinal optical (LO) phonon, is observed red-shifted by 26.5 meV from the ZPL, as commonly reported in the literature.[66,67] The ZPL shows an increase of the FWHM and a red shift with increasing temperature, the latter being characteristic for the temperature dependence of the band edge emission in most semiconductors.[68] In contrast, the Mn^{2+}:CdSe/CdS single QD exhibits a significantly broadened ZPL with a FWHM of 6.3 meV at 4 K. Interestingly, the phonon replica is shifted by 27.3 meV with respect to the ZPL and exhibits higher intensity compared to the undoped reference QD. This difference may indicate enhanced coupling between the LO phonon and the exciton, possibly related to the introduction of lattice distortions because of the doping and/or the specific shape of the nanocrystals (see Figure S1). Most important, the energy shift with temperature observed in the doped QD strongly deviates from its undoped counterpart, showing a blue shift between 4 and 40 K followed by a red shift when the temperature is further increased. In addition, a significant change of the emission line width is observed with raising temperature.

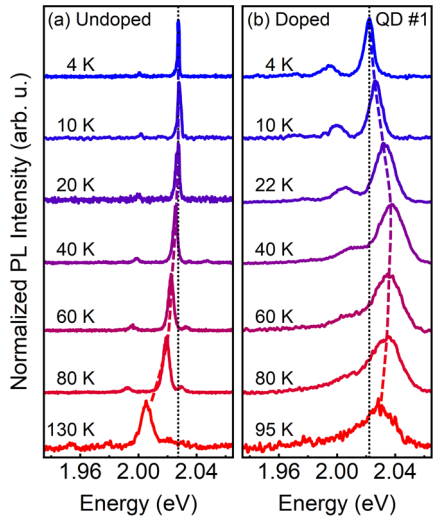

Figure 1. PL spectra of (a) an undoped CdSe/CdS single QD and (b) a single Mn^{2+}:CdSe/CdS doped QD (QD #1) at different temperatures. Dashed lines serve as a guide to the eye to indicate the shift of the emission maximum. Dotted lines mark the energy position of the ZPL at T = 4 K.

To investigate the temperature-dependent shift of the PL energy, ΔE_{PL}, of the single QDs more thoroughly, the peak energy values are extracted from the data in Figure 1 and summarized in Figure 2a. The undoped CdSe/CdS QD is discussed first to establish a reference for the intrinsic contributions to $\Delta E_{PL}(T)$, known as Varshni shift. To preclude statistical variations for the undoped reference, four individual undoped QDs were measured. The averaged data are displayed as gray dots in Figure 2a.

The temperature-dependent shift of the band gap for undoped semiconductors is commonly ascribed to a mixture of crystal volume expansion (minor influence) and electron−phonon interaction (major influence).[68] It is usually fit to fully empirical[68] or semi-empirical formulas, as introduced by O'Donnell and Chen:[71]

https://dx.doi.org/10.1021/acs.nanolett.9b05136
Nano Lett. 2020, 20, 1896−1906

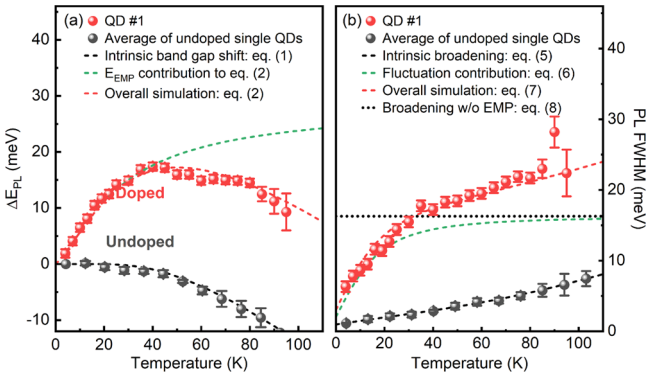

Figure 2. (a) Temperature-dependent PL shift ΔE_{PL} of QD #1 (red) and undoped single QDs (gray, averaged over four QDs). The dashed gray line indicates the fit of the data of undoped QDs to eq 1. The dashed red line shows the simulated overall shift for QD #1 described by eq 2. The green dashed curve illustrates the EMP contribution to eq 2. (b) ZPL FWHM of QD #1 (red) compared to the average of four undoped single QDs (gray). The data of undoped single QDs were fitted using eq 5 (black dashed curve). The red dashed curve shows the simulation result for QD #1, using eq 7 with the same parameters as used in (a). The contribution of the fluctuation broadening according to eq 6 is shown by the green dashed line. The high-temperature limit, that is, neglecting EMP formation, is calculated according to eq 8 and indicated as a black dotted line. The data of QD #1 in (a) and (b) were fitted simultaneously to eqs 2 and 7, using $N_0 = 17.82$ nm^3,[69] $N_0\alpha = 0.23$ eV,[70] and $N_0\beta = -1.27$ eV.[70]

$$W_{g,intrinsic}(T) = W_{g,intrinsic}(0\ K) - 2S_{OC}\langle\hbar\omega\rangle \frac{1}{\exp\left(\frac{\langle\hbar\omega\rangle}{k_B T}\right) - 1} \quad (1)$$

where $\Delta W_{g,intrinsic}(T) = W_{g,intrinsic}(T) - W_{g,intrinsic}(0\ K)$ is the energy shift of the band gap with respect to the value at 0 K, S_{OC} is a dimensionless coupling constant indicating the strength of the electron−phonon coupling, and $\langle\hbar\omega\rangle$ is an average phonon energy. Fitting the data of the undoped single QDs in Figure 2a to eq 1 yields $S_{OC} = 2.05$ and $\langle\hbar\omega\rangle = 14.2$ meV. These values are slightly smaller than those found in literature for bulk CdSe ($S_{OC,ref} = 2.5 \pm 0.4$, $\langle\hbar\omega\rangle_{ref} = 16.7 \pm 4.4$ meV, averaged over all CdSe values in ref 72), but are in good agreement with the trend discussed in ref 73 for CdSe QDs coated with large CdS shells.

$\Delta E_{PL}(T)$ of QD #1 is strikingly different from the behavior observed for undoped QDs, with an energy blue shift of 17 meV between 4 and 40 K (see red dots in Figure 2a), clearly deviating from the intrinsic red shift of the band gap with increasing temperature (see gray dots in Figure 2a). After a turnover between 40 and 70 K, the energy shift of the PL maximum of QD #1 starts to follow the red shift observed in the undoped analogue. Similar results in colloidal Mn^{2+}:CdSe nanocrystal ensembles have been interpreted as evidence of EMP formation.[31,32,35] In EMPs, the Mn^{2+} magnetic moments couple with the exciton spin via $sp-d$ exchange interactions, represented by the exchange field B_{exc}. Under the influence of B_{exc}, the Mn^{2+} spin ensemble is aligned with the exciton spin, leading to a spontaneous magnetization M_{Mn}, thus reducing the system's energy by the polaron energy E_{EMP}. As the temperature rises, thermal disorder and magnetic ordering compete against each other, weakening the magnetization and decreasing E_{EMP}, leading to a blue shift of the PL energy as observed here between 4 and 40 K.

The overall temperature-dependent energy shift of the PL maximum of the single Mn^{2+}:CdSe/CdS QD emission can thus be written as

$$\Delta E_{PL}(B, T) = \Delta W_{g,intrinsic}(T) + E_{EMP}(B, T) = \Delta W_{g,intrinsic}(T) - V_{eff} M_{Mn}(B, T) B_{exc} \quad (2)$$

where V_{eff} is the effective volume occupied by the exciton. The magnetization can be described with a modified Brillouin function for a paramagnetic spin ensemble and reads as

$$M_{Mn}(B, T) = x_{Mn} N_0 \mu_B g_{Mn} S_{eff} \mathcal{B}_{5/2}\left(\frac{5\mu_B g_{Mn}(B + B_{exc})}{2k_B(T_s + T_0)}\right) \quad (3)$$

where x_{Mn} is the dopant concentration, N_0 is the number of cations per volume, $\mathcal{B}_{5/2}$ is the Brillouin function for the Mn^{2+} $S = 5/2$ system, T_0 and $S_{eff} \leq 2.5$ are the antiferromagnetic temperature and the effective manganese spin, respectively, μ_B is the Bohr magneton, k_B is the Boltzmann constant, and $g_{Mn} = 2$ is the gyromagnetic ratio of Mn^{2+}. B and T are the experimentally controlled magnetic field and bath temperature, respectively. The spin temperature entering the magnetization is approximated by $T_s = T + \Delta T_s$, where ΔT_s is a zeroth-order correction accounting for the difference between the Mn^{2+} spin temperature and the bath temperature of the crystal. ΔT_s stems from heating of the Mn^{2+} spin ensemble, for example, due to spin−flip scattering between the optically generated electron−hole pairs and the Mn^{2+} spin system.[60,61] Using the commonly applied "exchange box" model, the exchange field can be written as[61,74]

$$B_{exc} = B_{exc}^{el} + B_{exc}^{h} = \frac{N_0\alpha - N_0\beta}{2V_{eff} N_0 g_{Mn} \mu_B} \quad (4)$$

where $N_0\alpha$ ($N_0\beta$) is the electron−dopant (hole−dopant) exchange constant and B_{exc}^{el} (B_{exc}^{h}) is the electron−dopant (hole−dopant) exchange field. Thus, inserting eqs 3 and 4 into eq 2 and using the parameters obtained from fitting the data of undoped QDs, the temperature dependence of ΔE_{PL} can be simulated, using V_{eff}, x_{Mn}, and ΔT_s as fit parameters.

In Figure 2a, the simulated data using the parameters $x_{Mn} = 1.73\%$, $V_{eff} = 30.4$ nm^3 (corresponding to an effective spherical exciton diameter of 3.9 nm), and $\Delta T_s = 4.3$ K are shown (red dashed curve). $T_0 = 1.1$ K and $S_{eff} = 2.3$ are obtained from interpolating data from ref 75. The calculations reproduce the experimental data (red symbols) very well. For clarity, the green dashed curve plots the EMP energy contribution to eq 2, with respect to the value at $T = 0$ K. The value of $x_{Mn} = 1.73\%$ is reasonable as an overall manganese concentration of 0.9% of the doped core−shell QDs has been measured via inductively coupled plasma atomic emission spectroscopy (ICP-AES), and the Mn^{2+} concentration varies statistically from dot to dot. Due to strong confinement of the hole wave function, the effective exciton volume should be approximately 36% of the core volume,[34] corresponding to $V_{eff,expected} = 35$ nm^3, in very good agreement with the value used in the simulation. From eq 4, these results yield an exchange field of $B_{exc} = 11.9$ T, which falls in the range (between 8 and 17 T) of values reported for similar Mn^{2+}:CdSe QDs.[31,32,34,35] The additional spin heating $\Delta T_s = 4.3$ K also closely resembles values found in literature (e.g., 4.4 K for self-assembled CdMnSe QDs[61] and 8 K − 14.5 K for self-assembled CdMnTe QDs[60]). For simplicity, we assume an overlap between the carrier wave functions with the doped regions equal to unity, which may result in a slight

https://dx.doi.org/10.1021/acs.nanolett.9b05136
Nano Lett. 2020, 20, 1896−1906

overestimation of the effective exciton volume, since the electron wave function is delocalized into the undoped CdS shell. Because the contribution of the $s-d$ exchange interaction is only about 15% of the total $sp-d$ exchange interaction, we estimate the error introduced by neglecting the finite overlap of the electron wave function with the magnetic dopants in deriving V_{eff} to be ≤10%. From this analysis, we conclude that $\Delta E_{PL}(T)$ of QD #1 is unambiguously correlated with the formation of an EMP. These results represent the first observation of an EMP in a single colloidal QD.

In Figure 2b, the extracted temperature-dependent FWHM of the undoped reference QD (gray dots) and QD #1 (red dots) are depicted. Again, the undoped reference is analyzed first to distinguish intrinsic line broadening effects from the contributions introduced by the dopants. Commonly, the change of the FWHM with temperature in undoped semiconductors is related to homogeneous broadening due to dephasing of the exciton by phonon scattering, as described by eq 5:[76]

$$\mathrm{FWHM}_{\mathrm{intrinsic}}(T) = \Gamma_0 + \Gamma_{AC}T + \Gamma_{LO}\frac{1}{\exp\left(\frac{\hbar\omega_{LO}}{k_B T}\right) - 1} \tag{5}$$

where Γ_0 is an inhomogeneous offset, for example, caused by a finite resolution of the experimental setup or by charge fluctuations, Γ_{AC} is a constant related to the coupling of the exciton to acoustic phonons, and Γ_{LO} describes coupling to the longitudinal optical phonons with energy $\hbar\omega_{LO}$. Because $\hbar\omega_{LO}$ = 26.5 meV is extracted directly from Figure 1, $\mathrm{FWHM}_{\mathrm{intrinsic}}(T)$ of the undoped QD can be fitted with the remaining three parameters (see black dashed curve in Figure 2b), yielding Γ_0 = 0.98 meV, Γ_{AC} = 49 μeV/K, and Γ_{LO} = 26.1 meV. These values are close to values found in literature for experiments on an ensemble of colloidal CdSe QDs (Γ_{AC} = 20 μeV/K and Γ_{LO} = 30 meV).[77] To the best of our knowledge, these parameters have not been reported for single colloidal CdSe QDs, so far.

Turning to the line broadening of QD #1, we find a distinct difference to the undoped reference, namely an enhanced emission line width and a strong increase of the broadening with temperature (see red dots in Figure 2b). More specifically, even at the lowest temperature (T = 4 K), the FWHM of QD #1 (~6.3 meV) exceeds the FWHM of the undoped reference (1.1 meV) considerably and increases very steeply with an anomalous negative curvature up to a FWHM of 17 meV at 40 K. In this temperature regime, the major contribution to the increase in FWHM for the undoped QDs is due to acoustic phonon scattering, leading to a line width broadening of just 1.7 meV with respect to the value measured at 4 K. For temperatures above 40 K, the slope of the FWHM(T) curve of QD #1 decreases, while even at 100 K, its FWHM still exceeds the undoped reference by almost a factor of 3.

Previously, a broadening of the ZPL line width in magnetically doped QDs grown by epitaxy has been correlated to statistical spin fluctuations within the Mn^{2+} ensemble.[63] These fluctuations stem from the statistically varying occupation of the six possible spin projections $s_{Mn,z}$ = ±5/2, ±3/2, ±1/2 of each individual Mn^{2+} ion, leading to fluctuations of the magnetization with variance $\langle M_{Mn}^2\rangle$. Considering the EMP equilibrium state and making use of the fluctuation dissipation theorem,[78] these fluctuations induce a broadening of the luminescence line width:[63]

$$\mathrm{FWHM}_{\mathrm{fluct}}(B, T) = \sqrt{8\ln(2)}\sqrt{k_B T_s B_{exc}^2 V_{eff}\left|\frac{dM_{Mn}(B, T)}{dB}\right|_{\substack{B_{exc}+B\\ T_s+T_0}}} \tag{6}$$

The total temperature dependence of the FWHM is now calculated in a first approximation by summing up the intrinsic contribution $\mathrm{FWHM}_{\mathrm{intrinsic}}(T)$ due to phonon broadening (obtained by fitting the data from the undoped reference to eq 5) and the contributions of spin fluctuations $\mathrm{FWHM}_{\mathrm{fluct}}(B,T)$:

$$\mathrm{FWHM}(B, T) = \mathrm{FWHM}_{\mathrm{intrinsic}}(T) + \mathrm{FWHM}_{\mathrm{fluct}}(B, T) \tag{7}$$

Importantly, no new parameters are introduced to describe the line width broadening of QD #1 with temperature. The red dashed curve in Figure 2b shows the result of simulating the line width according to eq 7 for QD #1 using the same parameters as for the simulation of $\Delta E_{PL}(T)$ (see Figure 2a), while the green and gray dashed curves show the contributions of $\mathrm{FWHM}_{\mathrm{fluct}}(T)$ and $\mathrm{FWHM}_{\mathrm{intrinsic}}(T)$, respectively. The precise measurement of $\Delta E_{PL}(T)$ and FWHM(T) in single Mn^{2+}-doped QDs makes it possible to use one parameter set to fit both energy shift and line width broadening over a large temperature range simultaneously with V_{eff}, x_{Mn}, and ΔT_s as the only fit parameters. An excellent agreement with the experiment is obtained, including the steep increase of the FWHM up to 40 K due to spin fluctuations. Note that in contrast to $\Delta E_{PL}(T)$, FWHM(T) is very sensitive to the parameter ΔT_s, essentially offsetting FWHM at 4 K. The observed negative curvature of FWHM(T) is revealed to be caused by the contribution of the Mn^{2+} magnetization fluctuations (green dashed curve), converging toward a value of 16.5 meV for temperatures above 80 K, where EMP formation is more and more suppressed by the thermal energy. The impact of statistical magnetic fluctuations on emission line widths in the absence of EMP formation, which can be caused either by too weak exchange interactions (i.e., low exchange fields, high temperatures) or by too fast exciton recombination, has been described for self-assembled QDs exhibiting small confinement and weak $sp-d$ exchange interactions.[79] In this case, the exciton recombination probes the instantaneous magnetization of the Mn^{2+} ensemble at the moment of photoexcitation. Since all possible spin projections $s_{Mn,z}$ = ±5/2, ±3/2, ±1/2 for each Mn^{2+} ion are probed with the same probability, the time average of the expectation value $\langle M_{Mn}\rangle$ is zero. However, the variance of the spin projections is nonzero with $\langle s_{Mn,z}^2\rangle$ = 35/12 for each Mn^{2+}. This variance leads to a finite variance $\langle M_{Mn}^2\rangle$ and therefore to a fluctuation broadening of the PL line width in the absence of EMP formation:[79]

$$\mathrm{FWHM}_{\mathrm{high}\text{-}T} = \sqrt{8\ln(2)}\frac{1}{N_0 V_{eff}}\sqrt{\frac{35}{12}x_{Mn}N_0 V_{eff}}\left(\frac{1}{2}N_0\alpha - \frac{1}{2}N_0\beta\right) \tag{8}$$

The black dotted line in Figure 2b represents the value calculated using eq 8 with the same parameters used in the simulations discussed above. Importantly, this formula implies no temperature dependence and can be regarded as the high temperature limit of eq 6.[80] At lower temperatures, the magnetic polaron in fact suppresses the fluctuation broadening due to spin alignment driven by the large exchange field B_{exc}.

To complete our picture of EMP formation and magnetization fluctuations in individual transition metal doped nanocrystals, single QD PL studies in an external magnetic field of variable strength and orientation have been performed.

https://dx.doi.org/10.1021/acs.nanolett.9b05136
Nano Lett. 2020, 20, 1896−1906

In Figure 3a,b magnetic field-dependent PL spectra of a second nanocrystal (QD #2) are shown for T = 4 K and T = 16 K,

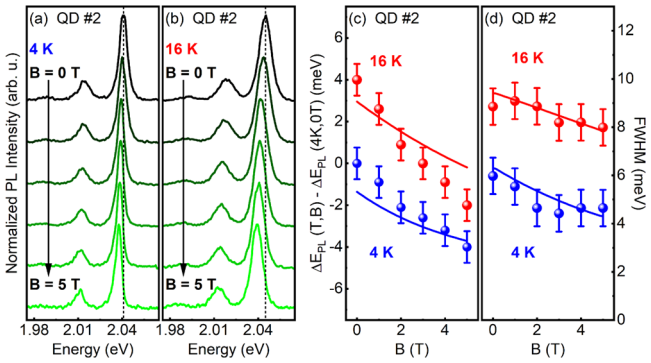

Figure 3. (a) Magnetic field-dependent PL spectra of QD #2 at (a) T = 4 K and (b) T = 16 K. The dashed lines are guides to the eye and mark the ZPL position at B = 0 T, while the magnetic field is varied up to B = 5 T in Faraday geometry. (c) Magnetic field-dependent energy shift $\Delta E_{PL}(B,T)$ with respect to the ZPL position at B = 0 T and T = 4 K and (d) magnetic field-dependent FWHM extracted from (a) and (b). Dots represent experimental data at T = 4 K (blue) and T = 16 K (red), and solid lines show results of a simultaneous fit of all four curves, using eqs 2 and 7.

respectively. Similar to QD #1, the ZPL of QD #2 also exhibits an energy blue shift and an increase in FWHM with rising temperature, indicating the observation of EMP formation. For both temperatures, the ZPL shifts to lower energies under the influence of a magnetic field, as highlighted by the dashed lines. The changes in energy and FWHM of the ZPL with magnetic field are extracted from the spectra and shown in Figure 3 c,d as blue and red dots for T = 4 K and T = 16 K, respectively. At B = 0 T, the blue shift ΔE_{PL} (~4.0 meV) and the line width increase ΔFWHM (~2.9 meV) between T = 4 K and T = 16 K are smaller than observed in QD #1. This comparison emphasizes the uniqueness of each individual QD with respect to, for example, dopant concentration and exciton volume (and thus exchange field).

Under the influence of an external magnetic field of B = 5 T in Faraday geometry, $E_{PL}(B)$ exhibits a red shift of $\Delta E_{PL}(B) \sim -4$ meV with respect to the B = 0 T value due to magnetic field-induced spin ordering.[58] This result indicates that in QD #2 the EMP exchange field is not strong enough to completely saturate M_{Mn} even at T = 4 K, because in the case of an extremely strong exchange field, the magnetization would be saturated and E_{EMP} would not depend on B. At T = 16 K, $E_{PL}(B)$ exhibits an enhanced red shift of $\Delta E_{PL}(B) = -6$ meV between B = 0 T and B = 5 T, since a higher temperature drives the magnetization further away from saturation, where the influence of the magnetic field on the spin ordering is larger. For the FWHM, a decrease with applied magnetic field is observed for both temperatures, which is consistent with partial suppression of spin fluctuations by increased magnetic order.

The data of $\Delta E_{PL}(B)$ and FWHM(B) can be fit to eqs 2 and 7 for both temperatures. Figure 3c,d shows the result of the simultaneous fit of all four curves, yielding x_{Mn} = 0.8%, ΔT_s = 5.8 K, and V_{eff} = 49 nm^3, corresponding to an effective spherical exciton diameter of 4.6 nm and B_{exc} = 7.3 T. It should be noted that not only the magnetic field dependence but, by considering the offset between the T = 4 K and T = 16 K curves, also the temperature dependence of $\Delta E_{PL}(B,T)$ and FWHM(B,T) are implicitly fitted as well. With these results, we demonstrate how an external magnetic field stabilizes EMP formation against thermal disorder, as reflected in the energy gain (red shift) and the narrowing of the FWHM.

Performing magneto-PL studies on several individual QDs reveals a surprising finding: Although usually a red shift with magnetic field is obtained at low temperatures, in some cases, the magnetic field has no effect or even causes a blue shift of the ZPL energy (see Supporting Information, Figure S5 for statistics). Figure 4a shows $\Delta E_{PL}(B)$ for three different single

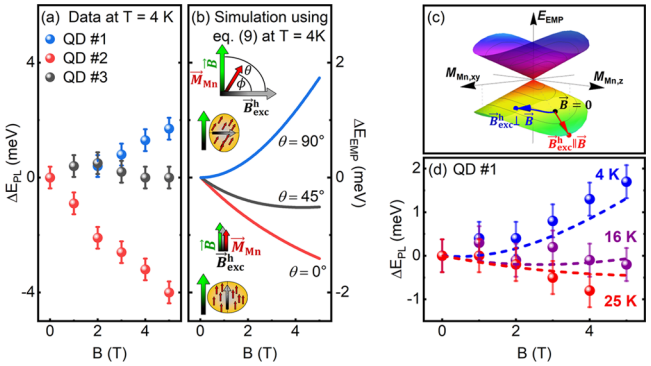

Figure 4. (a) PL energy shift with magnetic field in Faraday geometry for QDs #1, #2, and #3 at 4 K. (b) Simulation of the influence of the angle θ between the hole exchange field $\vec{B}^{h}_{exc}$ and the external magnetic field $\vec{B}$ using eq 9. The schematics illustrate the two limiting cases of a QD exhibiting a hole exchange field parallel (i.e., θ = 0°) and perpendicular (i.e., θ = 90°) to $\vec{B}$. In the latter case, the Mn^{2+} magnetization is directed along $\vec{B}^{h}_{exc} + \vec{B}$. (c) Schematic of the EMP energy surface, warped by an axial asymmetry into the z-direction, where contour lines represent lines of equal Mn^{2+} magnetization. Starting from the EMP equilibrium energy at $\vec{B}$ = 0 T (black dot), the influence of applying $\vec{B}$ parallel (red arrow) and perpendicular to the anisotropy axis (blue arrow) on the equilibrium EMP energy is illustrated. (d) ZPL energy shift between B = 0 T and B = 5 T in Faraday geometry for QD #1 (dots) at three different temperatures. Corresponding simulations are added (dashed lines) with the same fit parameters as extracted from Figure 2, now using eq 9 with θ = 80°.

QDs, measured at 4 K. Two of the QDs (QD #1 and QD #2) have already been discussed. While QD #2 shows a red shift, that is, a stabilization of its EMP with magnetic field (increased E_{EMP}), QD #3 shows no net shift between B = 0 and B = 5 T, and QD #1 shows a distinct blue shift, that is, a destabilization of the EMP in an external magnetic field (decreased E_{EMP}). Note that in the absence of EMP formation, increasing the magnetic field always leads to a red shift of the ZPL. Such red shifts stem from the giant Zeeman effect and are commonly observed in diluted magnetic semiconductors.[70]

The puzzling blue shift of the ZPL in Figure 4a cannot be explained with the theory presented so far. To resolve this discrepancy, the theoretical description needs to be generalized as follows: The magnetic moments of the Mn^{2+} ions can be aligned by both an external magnetic field $\vec{B}$ and the exchange field $\vec{B}_{exc} = \vec{B}^{el}_{exc} + \vec{B}^{h}_{exc}$ (see eq 3). The direction of $\vec{M}_{Mn}$ is then given by the direction of the total field $\vec{B}_{\Sigma} = \vec{B} + \vec{B}_{exc}$. In the isotropic case, it is usually assumed that electron and hole spin align along the direction determined by the instantaneous direction of the randomly fluctuating Mn^{2+} magnetization, which can be directed by an external magnetic field, and EMP

https://dx.doi.org/10.1021/acs.nanolett.9b05136
Nano Lett. 2020, 20, 1896−1906

formation occurs. Then, the directions of $\vec{M}_{Mn}$, $\vec{B}_{exc}^{el}$ and $\vec{B}_{exc}^{h}$ are expected to be colinear and given by the direction of $\vec{B}$ in the experimental situation, where the PL data are recorded by averaging over lots of excitation events. In that case, magnetic field, magnetization, and exchange field can be considered as scalars (eqs 2−4, 6, and 7).

If, however, exchange field and magnetization are not colinear, the full vector form of the above-mentioned equations needs to be used. This would imply an anisotropy in the nanocrystals, constraining, for example, the wave function of the hole, which is dominated by its anisotropic *p*-character. If a magnetic field $\vec{B} \perp \vec{B}_{exc}^{h}$ is applied, a strict constraining of the hole wave function in the direction of the anisotropy axis would result in $g_{\perp} = 0$. Such a behavior is, for example, known for the heavy hole in bulk CdSe in the wurtzite crystal structure,[69] where the *c*-axis forms the anisotropy axis. In literature, similar arguments have been used to explain the dependence of the PL polarization degree in undoped CdSe QDs on magnetic fields up to 60 T.[81,82] Under this assumption, the hole total angular momentum and thus the hole exchange field $\vec{B}_{exc}^{h}$ are not necessarily aligned along $\vec{B}$, and $\vec{M}_{Mn}$ is neither directed parallel to $\vec{B}_{exc}^{h}$ nor parallel to $\vec{B}$, but instead oriented along $\vec{B}_{\Sigma}$ (see cartoon in Figure 4b). Since the electron wave function is dominated by its isotropic *s*-character, we assume $\vec{B}_{exc}^{el} \| \vec{B}_{\Sigma}$. Then, the sum of $\vec{B}$ and $\vec{B}_{exc}^{h}$ dictates the direction of $\vec{B}_{\Sigma}$, and the modified EMP energy is given by[61]

$$E_{EMP}(\vec{B}, T) = -\vec{M}_{Mn} \cdot (\vec{B}_{exc}^{el} + \vec{B}_{exc}^{h}) V_{eff} = -V_{eff} |\vec{M}_{Mn}| (|\vec{B}_{exc}^{el}| + \cos(\phi) |\vec{B}_{exc}^{h}|) \quad (9)$$

where $\vec{M}_{Mn}(\vec{B}, T) = \vec{B}_{\Sigma}/B_{\Sigma} \cdot M_{Mn}(|\vec{B}_{\Sigma}|, T)$ is the modified version of eq 3 and ϕ the angle between $\vec{B}_{exc}^{h}$ and $\vec{M}_{Mn}$. Note that ϕ changes monotonically with increasing magnetic field strength if $\vec{B} \nparallel \vec{B}_{exc}^{h}$ and is therefore not easily accessible in an experiment. Therefore, in order to be compatible with the experimental situation, we define an angle θ between the external magnetic field $\vec{B}$ and the hole exchange field $\vec{B}_{exc}^{h}$ which does not change if the magnitude of the external field is varied. Figure 4b shows a simulation using the parameters previously extracted by fitting the temperature series of the emission of QD #1 (see Figure 2) for three different angles $\theta = 0°$, 45°, and 90°, that is, different orientations of the QD anisotropy axis with respect to the external magnetic field. For the simulations, x_{Mn}, ΔT_s, and V_{eff} as extracted for QD #1 (see Figure 2) are used. The simulation of $\Delta E_{PL}(B)$ in fact displays fundamental differences for different θ, namely a blue shift for $\theta = 90°$, no significant shift for $\theta = 45°$, and a red shift for $\theta = 0°$, in qualitative agreement with the data shown in Figure 4a. In contrast to the magnetic field-induced red shift of the ZPL energy explained above, a blue shift, that is, a *decrease* of the EMP binding energy, can only take place if $\vec{B}$ and $\vec{B}_{exc}^{h}$ are not collinear. Considering the angle dependence of eq 9, such a blue shift can be ascribed to the monotonic increase of ϕ with $|\vec{B}|$ (largest for $\theta = 90°$, i.e. $\vec{B} \perp \vec{B}_{exc}^{h}$), leading to a decreased projection of $\vec{B}_{exc}^{h}$ onto $\vec{M}_{Mn}$ (decrease of $\cos(\phi)$) and thus a decrease of the EMP binding energy E_{EMP} with $|\vec{B}|$.

Figure 4c illustrates the dependence of the EMP potential energy surface on $\vec{M}_{Mn}$, warped by an axial asymmetry, where, as an example, the anisotropy axis is chosen to be directed along the spatial *z* direction. In this example, the magnetization is not fully saturated at $\vec{B} = 0$ T after EMP formation, that is, the corresponding EMP equilibrium state (black dot) is not located on the outermost contour line. Applying a magnetic field $\vec{B}$ into the direction of the anisotropy axis enhances the magnetization $|\vec{M}_{Mn}|$ and thus causes the EMP equilibrium state to move *downhill* along the red arrow. Thus, a stabilization of the EMP state occurs due to an increase of the EMP binding energy by the applied field. While applying a magnetic field $\vec{B}$ perpendicular to the anisotropy axis also slightly enhances the magnetization, $\vec{M}_{Mn}$ is now directed along $\vec{B}_{\Sigma}$ and therefore displaced away from the anisotropy axis when $|\vec{B}|$ is increased. This causes the EMP equilibrium state to move uphill along the trace of the blue arrow, that is, a destabilization of the EMP state occurs due a reduction of the EMP binding energy. The observation of a magnetic field-induced blue shift, a missing energy shift, and a red shift of the ZPL energy in cases of QD #1, QD #2 and QD #3, respectively, may thus be assigned to the three cases of the individual QDs, having their anisotropy axes differently oriented with respect to the magnetic field direction. In colloidal QDs, a preferential axis for EMP formation has, to the best of our knowledge, not been observed so far, even though it has long been hypothesized to explain the EMP formation dynamics in Mn^{2+}-doped CdSe QDs.[31,32]

A second fundamental consequence of the directional dependence of eq 9 is the influence of temperature on the results of a magnetic field series. Recall that in the case of QD #2, where $\vec{B}_{exc}^{h}$ is parallel to $\vec{B}$ (or close to it), $d|\Delta E_{PL}|/dB$ increases with temperature (see Figure 3c) due to the fact that the increase in temperature drives the magnetization away from saturation, increasing the possible magnetization gain by application of $\vec{B}$. In contrast, in the case of QD #1, where $\vec{B}_{exc}^{h}$ is apparently almost perpendicular to $\vec{B}$, we find a fundamentally different behavior as shown in Figure 4c. Here, the blue shift with magnetic field observed at $T = 4$ K decreases with increasing temperature and turns into a red shift for $T \geq 25$ K. While, as discussed above, the influence of $\vec{B}$ on the magnetization gain (i.e., E_{EMP} gain) is temperature dependent, the evolution of ϕ and thus the projection term $|\vec{B}_{exc}^{h}|\cos(\phi)$ of $\vec{B}_{exc}^{h}$ onto $\vec{M}_{Mn}$ in eq 9 is temperature independent. Therefore, at low temperatures, where the magnetization is almost saturated, the projection term $|\vec{B}_{exc}^{h}|\cos(\phi)$ causes a destabilization of the EMP (blue shift) with external magnetic field. At higher temperatures, for example, $T > 25$ K, the projection term is overcompensated by the magnetization gain and $\vec{B}$ thus causes a net stabilization (red shift) of the EMP. In the picture of a warped potential energy surface (Figure 4c), the influence of a temperature increase is equivalent to moving the $\vec{B} = 0$ T equilibrium state (black dot) uphill in the direction of the $|\vec{M}_{Mn}| = 0$ origin. While the direction of $\vec{M}_{Mn}$ is still displaced away from the anisotropy axis, the application of $\vec{B}$ perpendicular to the anisotropy axis increases $|\vec{M}_{Mn}|$ and causes a net gain in E_{EMP}, that is, a downhill movement.

Using eq 9 with the same parameters for x_{Mn}, V_{eff}, and ΔT_s as extracted from the temperature series depicted in Figure 2, we simulated the theoretical behavior of QD #1 in a magnetic

https://dx.doi.org/10.1021/acs.nanolett.9b05136
Nano Lett. 2020, 20, 1896−1906

field at three different temperatures using $\theta = 80°$. The results, displayed as dashed lines in Figure 4 (c), resemble the trend of the data very well, demonstrating the strength of the model and underlining the physical considerations about the origin of this effect.

To directly test our hypothesis of an anisotropy axis constraining the direction of the hole exchange field in the nanocrystals, we use the possibility of our experimental setup to apply a rotating (3D) magnetic field with $|\vec{B}| = 2$ T in any direction with respect to the substrate surface. In the case of a uniaxial anisotropy, a red shift (stabilization) and a blue shift (destabilization) would be expected if the magnetic field is aligned parallel and perpendicular to the axis of anisotropy, respectively. In this case, the full 3D dependence of EMP formation on the direction of the magnetic field is characterized by the projection angle ϕ of $\vec{M}_{Mn}$ onto $\vec{B}^{h}_{exc}$, or equivalently, by the angle θ between $\vec{B}^{h}_{exc}$ and $\vec{B}$, as introduced above. For these experiments, we define a plane given by the direction of the anisotropy axis (i.e., direction of the maximum red shift) and the direction where the maximum blue shift is observed (i.e., a direction perpendicular to the anisotropy axis), and we then rotate $\vec{B}$ within this plane. Figure 5 illustrates the

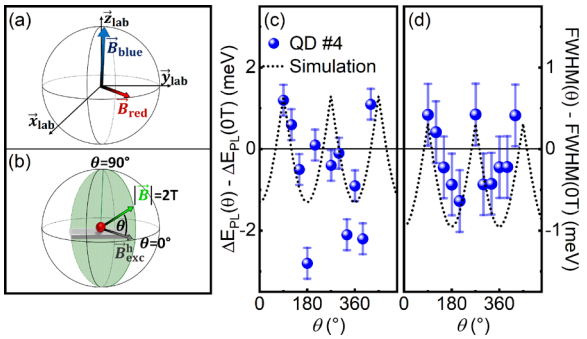

Figure 5. (a) Illustration of the rotating magnetic field experiment on QD #4. The QD ZPL energy shows a maximum blue shift with respect to $|\vec{B}| = 0$ T when applying a magnetic field $\vec{B}$ close to the $[x = 0, y = 0, z = 1]$ direction in lab coordinates. Rotating the magnetic field perpendicular to [0,0,1] leads to a red shift of the ZPL energy with respect to $|\vec{B}| = 0$ T, which is maximized for the [1,1,0] direction. (b) Schematic of the angle-dependent magneto PL measurement on a single anisotropic QD (red dot). The previously found directions of maximum red shift ([1,1,0]), i.e. the presumed direction of $\vec{B}^{h}_{exc}$, and maximum blue shift (close to [0,0,1]) are used to span the plane (green shaded) in which the magnetic field with $|\vec{B}| = 2$ T is rotated.. The rotation is characterized by the angle θ between $\vec{B}$ and the [1,1,0] direction. (c) ZPL energy shift and (d) change of FWHM of QD #4 with respect to $|\vec{B}| = 0$ T when rotating $\vec{B}(\theta)$ in the plane spanned by the lab [1,1,0] and [0,0,1] directions. $|\vec{B}| = 2$ T and $T = 4$ K are kept constant during the experiment. Dotted black lines show simulations using eqs 9 and 10 with $x_{Mn} = 2\%$, $V_{eff} = 58$ nm^3, and $\Delta T_s = 0$ K.

rotating magnetic field experiment for single QD #4 (see Supporting Information, Figure S6, for more statistics). As depicted in Figure 5a, the maximum blue and red shifts of the ZPL position with respect to $|\vec{B}| = 0$ T were found when the magnetic field was applied close to the $[x_{lab} = 0, y_{lab} = 0, z_{lab} = 1]$ and [1,1,0] directions, respectively, for QD #4. These directions were used to define the plane in which the magnetic field with $|\vec{B}| = 2$ T was rotated (green shaded plane in Figure 5b).

Figure 5c,d shows the evolution of the ZPL shift $\Delta E_{PL}(\theta)$ and the change in line width $\Delta FWHM(\theta)$ with respect to $|\vec{B}| = 0$ T as the magnetic field is rotated. Starting from $\theta = 90°$, the energy shift $\Delta E_{PL}(\theta)$ follows the progression blue−red−blue with rising θ with a periodicity of $\Delta\theta = 180°$. With the same periodicity, the change in FWHM evolves from a broadening to a narrowing to a broadening and so forth. We interpret these findings as an angle-dependent stabilization and destabilization of EMP formation. Hereby, the stabilization, that is, an enhancement of the EMP binding energy and a suppression of the magnetic fluctuations, is maximized if the magnetic field is coaxial with the anisotropy axis ($\theta = 0°$ or 180°). A destabilization, that is, a reduced EMP binding energy and an enhanced fluctuation broadening, occurs if the magnetic field and anisotropy axes are perpendicular. Interestingly, the 180° periodicity implies an abrupt reorientation of the direction of the hole exchange field by 180°, and thus a change in EMP formation direction, as soon as the projection of $\vec{B}$ on the anisotropy axis changes its sign, that is, at $\theta = 90°$ and 270°.

To model this behavior, we use eq 9 and a generalized version of eq 6, including the influence of transverse and longitudinal magnetization fluctuations with respect to the exchange field:[61]

$$FWHM_{fluct}(\vec{B}, T) = \sqrt{8\ln(2)} \cdot \sqrt{V_{eff}[(|\vec{B}^{el}_{exc}| + |\vec{B}^{h}_{exc}|\cos(\phi))^2\langle\delta M_{\parallel}^2\rangle + (|\vec{B}^{h}_{exc}|\sin(\phi))^2\langle\delta M_{\perp}^2\rangle]} \quad (10)$$

The longitudinal and transverse fluctuations of the magnetization are given by[61]

$$\langle\delta M_{\parallel}^2\rangle = \left|\frac{dM_{Mn,\parallel}(\vec{B}, T)}{dB_{\parallel}}\right|_{\vec{B}_{\Sigma}} k_B T_s = \left|\frac{dM_{Mn}(B, T)}{dB}\right|_{|\vec{B}_{\Sigma}|} k_B T_s$$

$$\langle\delta M_{\perp}^2\rangle = \left|\frac{dM_{Mn,\perp}(\vec{B}, T)}{dB_{\perp}}\right|_{\vec{B}_{\Sigma}} k_B T_s = \frac{|\vec{M}_{Mn}(\vec{B})|}{|\vec{B}_{\Sigma}|} k_B T_s \quad (11)$$

Figure 5c,d exhibits the simulations of $\Delta E_{PL}(\theta)$ and $\Delta FWHM(\theta)$ for QD #4 as dotted lines using $x_{Mn} = 2\%$, $\Delta T_s = 0$ K, $V_{eff} = 58$ nm^3 (corresponding to an effective spherical exciton diameter of 4.8 nm and $|\vec{B}_{exc}| = 6.3$ T at $\vec{B} = 0$ T). Note that at $\theta = 90°$ and 270°, this corresponds to a maximum angle of $\phi = 20°$ between $\vec{M}$ and $\vec{B}^{h}_{exc}$. The simulations show good qualitative agreement with the experimental data and reproduce well the trend of switching between EMP stabilization and EMP destabilization via the angle of the external magnetic field with respect to the anisotropy axis of the QD. Apparently, EMP formation can be directed by a magnetic field much smaller than the exchange field.

The conclusion from this analysis of an anisotropy axis constraining the direction of the hole wave function is consistent with previous work,[81,82] where, for example, in undoped CdSe QDs, magnetic fields up to 60 T were found to be insufficient to reach a PL polarization degree higher than 75%.[81] The results presented here unambiguously prove the existence of an anisotropy axis in our doped colloidal QDs, and they highlight the major importance of this anisotropy for EMP formation. Such anisotropy has been invoked to explain EMP formation-reorientation dynamics[31] and the finite

https://dx.doi.org/10.1021/acs.nanolett.9b05136
Nano Lett. 2020, 20, 1896−1906

maximum PL polarization[32] of colloidal magnetically doped QDs, but has never previously been identified experimentally. The most prominent sources of anisotropy in QDs are the ones introduced by the wurtzite crystal lattice with an energy splitting $\Delta_{int} \approx 24$ meV[83] and the shape anisotropy due to distortions of the spherical QD shape with an energy splitting Δ_{sh}. While the former is a uniaxial anisotropy, the latter may include more than one symmetry axes and is dependent on the magnitude of the distortion (i.e., the ellipticity in the case of a uniaxial distortion) and the QD size. In our case, the Mn^{2+}:CdSe cores are only slightly ellipsoidal (see Supporting Information Figure S1), so that we expect $\Delta_{int} > \Delta_{sh}$ for the investigated QDs with core diameter of 5.9 nm.[83] Additionally, the magnetic field-dependent PL energy shift shown in Figure 5 hints toward a periodicity of $\Delta\theta = 180°$, that is, a uniaxial symmetry rather than a triangular ($\Delta\theta = 120°$) or multi-axial symmetry. Although we cannot reliably identify the main source of the anisotropy, we therefore hypothesize the crystal asymmetry of the wurtzite lattice to be the main source for constraining the direction of the hole wave function.

Conclusion. In summary, temperature and magnetic field-dependent confocal PL spectroscopy was used to unravel the formation of EMPs in single colloidal QDs for the first time. The absence of a statistical variation of size, shape and crystal orientation—typical in an ensemble of nanocrystals—provides unique insights into the role of anisotropy in EMP formation and magnetic fluctuations. The single QD PL line width is strongly influenced by fluctuations of the Mn^{2+} spin ensemble, leading to an unusually steep increase of the FWHM with temperature. Detailed modeling of the temperature-dependent ZPL energy shifts and the corresponding line width broadening allows extraction of key parameters including V_{eff}, x_{Mn}, and spin heating ΔT_s for single QDs. Experiments in a 3D vector magnetic field reveal both stabilization and destabilization of the EMP that are unique for each single QD and that are reflected by a corresponding change in energy and FWHM of the ZPL depending on the direction of the applied magnetic field. QD anisotropy was identified as the source of this behavior, constraining the direction of the hole exchange field within the QD and consequently directing the orientation of EMP formation. Our findings not only demonstrate the fundamental impact of anisotropy on the physical properties of doped colloidal nanocrystals but also indicate a promising pathway to control the directionality of optically generated magnetism in colloidal nanocrystals.

Methods. *μ-PL Spectroscopy.* μ-PL spectra were recorded using a confocal microscopy setup (Attocube attoCFM I, microscope LT-APO-Vis, NA: 0.82), inserted into a closed cycle cryostat (T_{sample} = 4.0 K) with the option to apply magnetic fields up to 5 T in Faraday geometry or, alternatively, up to 2 T in any arbitrary direction. The sample is surrounded by He exchange gas, ensuring the thermal coupling between the QDs and the environment. Optical excitation was conducted with a 532 nm solid-state laser (Laserglow LRS-0532 DPSS) in combination with a laser clean up filter (Thorlabs FLH532-10) and an ultrasteep long-pass edge filter (Razor Edge 532-RU), using excitation power densities of <10 W/cm^{-2}. Spectra were recorded using a liquid nitrogen-cooled charge coupled device (CCD) camera (Horiba Symphony II, back illuminated deep depletion 1-LS) in combination with monochromator setup (Horiba Triax 550), equipped with a 600 mm^{-1} grating. Integration time for all measurements was held constant at 300 s.

■ ASSOCIATED CONTENT

Supporting Information

The Supporting Information is available free of charge at https://pubs.acs.org/doi/10.1021/acs.nanolett.9b05136.

Quantum dot synthesis, analysis, and preparation. PL spectra used in Figures 4 and 5 (PDF)

■ AUTHOR INFORMATION

Corresponding Author

Rachel Fainblat − *Werkstoffe der Elektrotechnik and CENIDE, University of Duisburg-Essen, Duisburg 47057, Germany;* orcid.org/0000-0002-9488-2563; Email: Rachel.fainblat-padua@uni-due.de

Authors

Severin Lorenz − *Werkstoffe der Elektrotechnik and CENIDE, University of Duisburg-Essen, Duisburg 47057, Germany*

Christian S. Erickson − *Department of Chemistry, University of Washington, Seattle, Washington 98195-1700, United States;* orcid.org/0000-0001-7888-0034

Maurizio Riesner − *Werkstoffe der Elektrotechnik and CENIDE, University of Duisburg-Essen, Duisburg 47057, Germany*

Daniel R. Gamelin − *Department of Chemistry, University of Washington, Seattle, Washington 98195-1700, United States;* orcid.org/0000-0003-2888-9916

Gerd Bacher − *Werkstoffe der Elektrotechnik and CENIDE, University of Duisburg-Essen, Duisburg 47057, Germany;* orcid.org/0000-0001-8419-2158

Complete contact information is available at: https://pubs.acs.org/10.1021/acs.nanolett.9b05136

Notes

The authors declare no competing financial interest.

■ ACKNOWLEDGMENTS

S.L., R.F., and G.B. acknowledge the Deutsche Forschungsgemeinschaft (DFG) under contracts BA 1422/13-2 and BA 1422/19. We thank N. Stracke for the preparation of the patterned substrates by e-beam lithography and J. Klein for the assistance during preparation of the TOC graphic. This research was partially supported by the US National Science Foundation (NSF) through project DMR-1807394 (to D.R.G.). Additional support from the US NSF through the UW Molecular Engineering Materials Center, a Materials Research Science and Engineering Center (DMR-1807394 and DMR-1719797), is gratefully acknowledged.

■ REFERENCES

(1) Kovalenko, M. V.; Manna, L.; Cabot, A.; Hens, Z.; Talapin, D. V.; Kagan, C. R.; Klimov, V. I.; Rogach, A. L.; Reiss, P.; Milliron, D. J.; et al. Prospects of Nanoscience with Nanocrystals. *ACS Nano* **2015**, *9*, 1012−1057.

(2) Pietryga, J. M.; Park, Y.-S.; Lim, J.; Fidler, A. F.; Bae, W. K.; Brovelli, S.; Klimov, V. I. Spectroscopic and Device Aspects of Nanocrystal Quantum Dots. *Chem. Rev.* **2016**, *116*, 10513−10622.

(3) Erwin, S. C.; Zu, L.; Haftel, M. I.; Efros, A. L.; Kennedy, T. A.; Norris, D. J. Doping Semiconductor Nanocrystals. *Nature* **2005**, *436*, 91−94.

(4) Norris, D. J.; Efros, A. L.; Erwin, S. C. Doped Nanocrystals. *Science* **2008**, *319*, 1776−1779.

(5) Beaulac, R.; Ochsenbein, S. T.; Gamelin, D. R. Colloidal Transition-Metal-Doped Quantum Dots. In *Nanocrystal Quantum*

Dots; Klimov, V. I., Ed.; CRC Press: Boca Raton, FL, 2010; pp 397–453.
(6) Vlaskin, V. A.; Barrows, C. J.; Erickson, C. S.; Gamelin, D. R. Nanocrystal Diffusion Doping. *J. Am. Chem. Soc.* **2013**, *135*, 14380–14389.
(7) Suyver, J. F.; Wuister, S. F.; Kelly, J. J.; Meijerink, A. Luminescence of Nanocrystalline ZnSe:Mn^{2+}. *Phys. Chem. Chem. Phys.* **2000**, *2*, 5445–5448.
(8) Beaulac, R.; Archer, P. I.; Gamelin, D. R. Luminescence in Colloidal Mn^{2+}-Doped Semiconductor Nanocrystals. *J. Solid State Chem.* **2008**, *181*, 1582–1589.
(9) Karan, N. S.; Sarma, D. D.; Kadam, R. M.; Pradhan, N. Doping Transition Metal (Mn or Cu) Ions in Semiconductor Nanocrystals. *J. Phys. Chem. Lett.* **2010**, *1*, 2863–2866.
(10) Erickson, C. S.; Bradshaw, L. R.; McDowall, S.; Gilbertson, J. D.; Gamelin, D. R.; Patrick, D. L. Zero-Reabsorption Doped-Nanocrystal Luminescent Solar Concentrators. *ACS Nano* **2014**, *8*, 3461–3467.
(11) Knowles, K. E.; Nelson, H. D.; Kilburn, T. B.; Gamelin, D. R. Singlet–Triplet Splittings in the Luminescent Excited States of Colloidal Cu^+:CdSe, Cu^+:InP, and $CuInS_2$ Nanocrystals: Charge-Transfer Configurations and Self-Trapped Excitons. *J. Am. Chem. Soc.* **2015**, *137*, 13138–13147.
(12) Parobek, D.; Roman, B. J.; Dong, Y.; Jin, H.; Lee, E.; Sheldon, M.; Son, D. H. Exciton-to-Dopant Energy Transfer in Mn-Doped Cesium Lead Halide Perovskite Nanocrystals. *Nano Lett.* **2016**, *16*, 7376–7380.
(13) Pu, C.; Ma, J.; Qin, H.; Yan, M.; Fu, T.; Niu, Y.; Yang, X.; Huang, Y.; Zhao, F.; Peng, X. Doped Semiconductor-Nanocrystal Emitters with Optimal Photoluminescence Decay Dynamics in Microsecond to Millisecond Range: Synthesis and Applications. *ACS Cent. Sci.* **2016**, *2*, 32–39.
(14) Liu, W.; Lin, Q.; Li, H.; Wu, K.; Robel, I.; Pietryga, J. M.; Klimov, V. I. Mn^{2+}-Doped Lead Halide Perovskite Nanocrystals with Dual-Color Emission Controlled by Halide Content. *J. Am. Chem. Soc.* **2016**, *138*, 14954–14961.
(15) Sharma, M.; Gungor, K.; Yeltik, A.; Olutas, M.; Guzelturk, B.; Kelestemur, Y.; Erdem, T.; Delikanli, S.; McBride, J. R.; Demir, H. V. Near-Unity Emitting Copper-Doped Colloidal Semiconductor Quantum Wells for Luminescent Solar Concentrators. *Adv. Mater.* **2017**, *29*, 1700821.
(16) Nelson, H. D.; Hinterding, S. O. M.; Fainblat, R.; Creutz, S. E.; Li, X.; Gamelin, D. R. Mid-Gap States and Normal vs Inverted Bonding in Luminescent Cu^+- and Ag^+-Doped CdSe Nanocrystals. *J. Am. Chem. Soc.* **2017**, *139*, 6411–6421.
(17) Norris, D. J.; Yao, N.; Charnock, F. T.; Kennedy, T. A. High-Quality Manganese-Doped ZnSe Nanocrystals. *Nano Lett.* **2001**, *1*, 3–7.
(18) Beaulac, R.; Archer, P. I.; Ochsenbein, S. T.; Gamelin, D. R. Mn^{2+}-Doped CdSe Quantum Dots: New Inorganic Materials for Spin-Electronics and Spin-Photonics. *Adv. Funct. Mater.* **2008**, *18*, 3873–3891.
(19) Bussian, D. A.; Crooker, S. A.; Yin, M.; Brynda, M.; Efros, A. L.; Klimov, V. I. Tunable Magnetic Exchange Interactions in Manganese-Doped Inverted Core–Shell ZnSe–CdSe Nanocrystals. *Nat. Mater.* **2009**, *8*, 35–40.
(20) Barrows, C. J.; Vlaskin, V. A.; Gamelin, D. R. Absorption and Magnetic Circular Dichroism Analyses of Giant Zeeman Splittings in Diffusion-Doped Colloidal $Cd_{1-x}Mn_xSe$ Quantum Dots. *J. Phys. Chem. Lett.* **2015**, *6*, 3076–3081.
(21) Yang, J.; Fainblat, R.; Kwon, S. G.; Muckel, F.; Yu, J. H.; Terlinden, H.; Kim, B. H.; Iavarone, D.; Choi, M. K.; Kim, I. Y.; et al. Route to the Smallest Doped Semiconductor: Mn^{2+}-Doped $(CdSe)_{13}$ Clusters. *J. Am. Chem. Soc.* **2015**, *137*, 12776–12779.
(22) Delikanli, S.; Akgul, M. Z.; Murphy, J. R.; Barman, B.; Tsai, Y.; Scrace, T.; Zhang, P.; Bozok, B.; Hernández-Martínez, P. L.; Christodoulides, J.; et al. Mn^{2+}-Doped CdSe/CdS Core/Multishell Colloidal Quantum Wells Enabling Tunable Carrier–Dopant Exchange Interactions. *ACS Nano* **2015**, *9*, 12473–12479.
(23) Yang, J.; Muckel, F.; Baek, W.; Fainblat, R.; Chang, H.; Bacher, G.; Hyeon, T. Chemical Synthesis, Doping, and Transformation of Magic-Sized Semiconductor Alloy Nanoclusters. *J. Am. Chem. Soc.* **2017**, *139*, 6761–6770.
(24) Yang, J.; Muckel, F.; Choi, B. K.; Lorenz, S.; Kim, I. Y.; Ackermann, J.; Chang, H.; Czerney, T.; Kale, V. S.; Hwang, S. J.; et al. Co^{2+}-Doping of Magic-Sized CdSe Clusters: Structural Insights via Ligand Field Transitions. *Nano Lett.* **2018**, *18*, 7350–7357.
(25) Muckel, F.; Delikanli, S.; Hernández-Martínez, P. L.; Priesner, T.; Lorenz, S.; Ackermann, J.; Sharma, M.; Demir, H. V.; Bacher, G. *sp–d* Exchange Interactions in Wave Function Engineered Colloidal CdSe/Mn:CdS Hetero-Nanoplatelets. *Nano Lett.* **2018**, *18*, 2047–2053.
(26) Furdyna, J. K. Diluted Magnetic Semiconductors. *J. Appl. Phys.* **1988**, *64*, R29–R64.
(27) *Semiconductors and Semimetals*; Furdyna, J. K., Kossut, J., Eds.; Academic Press, Inc.: San Diego, 1972; Vol. *25*.
(28) Hoffman, D. M.; Meyer, B. K.; Ekimov, A. I.; Merkulov, I. A.; Efros, A. L.; Rosen, M.; Couino, G.; Gacoin, T.; Boilot, J. P. Giant Internal Magnetic Fields in Mn Doped Nanocrystal Quantum Dots. *Solid State Commun.* **2000**, *114*, 547–550.
(29) Fainblat, R.; Frohleiks, J.; Muckel, F.; Yu, J. H.; Yang, J.; Hyeon, T.; Bacher, G. Quantum Confinement-Controlled Exchange Coupling in Manganese(II)-Doped CdSe Two-Dimensional Quantum Well Nanoribbons. *Nano Lett.* **2012**, *12*, 5311–5317.
(30) Muckel, F.; Yang, J.; Lorenz, S.; Baek, W.; Chang, H.; Hyeon, T.; Bacher, G.; Fainblat, R. Digital Doping in Magic-Sized CdSe Clusters. *ACS Nano* **2016**, *10*, 7135–7141.
(31) Beaulac, R.; Schneider, L.; Archer, P. I.; Bacher, G.; Gamelin, D. R. Light-Induced Spontaneous Magnetization in Doped Colloidal Quantum Dots. *Science* **2009**, *325*, 973–976.
(32) Nelson, H. D.; Bradshaw, L. R.; Barrows, C. J.; Vlaskin, V. A.; Gamelin, D. R. Picosecond Dynamics of Excitonic Magnetic Polarons in Colloidal Diffusion-Doped $Cd_{1-x}Mn_xSe$ Quantum Dots. *ACS Nano* **2015**, *9*, 11177–11191.
(33) Rice, W. D.; Liu, W.; Baker, T. A.; Sinitsyn, N. A.; Klimov, V. I.; Crooker, S. A. Revealing Giant Internal Magnetic Fields Due to Spin Fluctuations in Magnetically Doped Colloidal Nanocrystals. *Nat. Nanotechnol.* **2016**, *11*, 137–142.
(34) Rice, W. D.; Liu, W.; Pinchetti, V.; Yakovlev, D. R.; Klimov, V. I.; Crooker, S. A. Direct Measurements of Magnetic Polarons in $Cd_{1-x}Mn_xSe$ Nanocrystals from Resonant Photoluminescence. *Nano Lett.* **2017**, *17*, 3068–3075.
(35) Muckel, F.; Barrows, C. J.; Graf, A.; Schmitz, A.; Erickson, C. S.; Gamelin, D. R.; Bacher, G. Current-Induced Magnetic Polarons in a Colloidal Quantum-Dot Device. *Nano Lett.* **2017**, *17*, 4768–4773.
(36) Bhattacharjee, A. K. Crystal-Field Model for Acceptor-Associated Bound Magnetic Polarons in Wurtzite Semiconductors. *Phys. Rev. B: Condens. Matter Mater. Phys.* **1987**, *35*, 9108–9111.
(37) Peng, B.; May, J. W.; Gamelin, D. R.; Li, X. Effects of Crystallographic and Shape Anisotropies on Dopant-Carrier Exchange Interactions in Magnetic Semiconductor Quantum Dots. *J. Phys. Chem. C* **2014**, *118*, 7630–7636.
(38) Hazarika, A.; Layek, A.; De, S.; Nag, A.; Debnath, S.; Mahadevan, P.; Chowdhury, A.; Sarma, D. D. Ultranarrow and Widely Tunable Mn^{2+}-Induced Photoluminescence from Single Mn-Doped Nanocrystals of ZnS-CdS Alloys. *Phys. Rev. Lett.* **2013**, *110*, 267401.
(39) Ishizumi, A.; Kanemitsu, Y. Blinking Behavior of Surface-Defect and Impurity Luminescence in Nondoped and Mn^{2+}-Doped CdS Nanocrystals. *J. Phys. Soc. Jpn.* **2009**, *78*, 083705.
(40) Zhang, Y.; Gan, C.; Muhammad, J.; Battaglia, D.; Peng, X.; Xiao, M. Enhanced Fluorescence Intermittency in Mn-Doped Single ZnSe Quantum Dots. *J. Phys. Chem. C* **2008**, *112*, 20200–20205.
(41) Whitham, P. J.; Knowles, K. E.; Reid, P. J.; Gamelin, D. R. Photoluminescence Blinking and Reversible Electron Trapping in Copper-Doped CdSe Nanocrystals. *Nano Lett.* **2015**, *15*, 4045–4051.
(42) Fainblat, R.; Barrows, C. J.; Hopmann, E.; Siebeneicher, S.; Vlaskin, V. A.; Gamelin, D. R.; Bacher, G. Giant Excitonic Exchange

https://dx.doi.org/10.1021/acs.nanolett.9b05136
Nano Lett. 2020, 20, 1896–1906

Splittings at Zero Field in Single Colloidal CdSe Quantum Dots Doped with Individual Mn^{2+} Impurities. *Nano Lett.* **2016**, *16*, 6371−6377.
(43) Nirmal, M.; Dabbousi, B. O.; Bawendi, M. G.; Macklin, J. J.; Trautman, J. K.; Harris, T. D.; Brus, L. E. Fluorescence Intermittency in Single Cadmium Selenide Nanocrystals. *Nature* **1996**, *383*, 802−804.
(44) Chen, Y.; Vela, J.; Htoon, H.; Casson, J. L.; Werder, D. J.; Bussian, D. A.; Klimov, V. I.; Hollingsworth, J. A. "Giant" Multishell CdSe Nanocrystal Quantum Dots with Suppressed Blinking. *J. Am. Chem. Soc.* **2008**, *130*, 5026−5027.
(45) Schlegel, G.; Bohnenberger, J.; Potapova, I.; Mews, A. Fluorescence Decay Time of Single Semiconductor Nanocrystals. *Phys. Rev. Lett.* **2002**, *88*, 137401.
(46) Neuhauser, R. G.; Shimizu, K. T.; Woo, W. K.; Empedocles, S. A.; Bawendi, M. G. Correlation between Fluorescence Intermittency and Spectral Diffusion. *Phys. Rev. Lett.* **2000**, *85*, 3301−3304.
(47) Efros, A. L.; Nesbitt, D. J. Origin and Control of Blinking in Quantum Dots. *Nat. Nanotechnol.* **2016**, *11*, 661−671.
(48) Empedocles, S. A. Quantum-Confined Stark Effect in Single CdSe Nanocrystallite Quantum Dots. *Science* **1997**, *278*, 2114−2117.
(49) Fernée, M. J.; Sinito, C.; Tamarat, P.; Lounis, B. State Selective Pumping Reveals Spin-Relaxation Pathways in CdSe Quantum Dots. *Nano Lett.* **2014**, *14*, 4480−4485.
(50) Sinito, C.; Fernée, M. J.; Goupalov, S. V.; Mulvaney, P.; Tamarat, P.; Lounis, B. Tailoring the Exciton Fine Structure of Cadmium Selenide Nanocrystals with Shape Anisotropy and Magnetic Field. *ACS Nano* **2014**, *8*, 11651−11656.
(51) Osovsky, R.; Cheskis, D.; Kloper, V.; Sashchiuk, A.; Kroner, M.; Lifshitz, E. Continuous-Wave Pumping of Multiexciton Bands in the Photoluminescence Spectrum of a Single CdTe-CdSe Core-Shell Colloidal Quantum Dot. *Phys. Rev. Lett.* **2009**, *102*, 197401.
(52) Shulenberger, K. E.; Bischof, T. S.; Caram, J. R.; Utzat, H.; Coropceanu, I.; Nienhaus, L.; Bawendi, M. G. Multiexciton Lifetimes Reveal Triexciton Emission Pathway in CdSe Nanocrystals. *Nano Lett.* **2018**, *18*, 5153−5158.
(53) Besombes, L.; Léger, Y.; Maingault, L.; Ferrand, D.; Mariette, H.; Cibert, J. Probing the Spin State of a Single Magnetic Ion in an Individual Quantum Dot. *Phys. Rev. Lett.* **2004**, *93*, 207403.
(54) Léger, Y.; Besombes, L.; Maingault, L.; Mariette, H. Valence-Band Mixing in Neutral, Charged, and Mn-Doped Self-Assembled Quantum Dots. *Phys. Rev. B: Condens. Matter Mater. Phys.* **2007**, *76*, 045331.
(55) Kobak, J.; Smoleński, T.; Goryca, M.; Papaj, M.; Gietka, K.; Bogucki, A.; Koperski, M.; Rousset, J. G.; Suffczyński, J.; Janik, E.; et al. Designing Quantum Dots for Solotronics. *Nat. Commun.* **2014**, *5*, 3191.
(56) Smoleński, T.; Kazimierczuk, T.; Kobak, J.; Goryca, M.; Golnik, A.; Kossacki, P.; Pacuski, W. Magnetic Ground State of an Individual Fe^{2+} Ion in Strained Semiconductor Nanostructure. *Nat. Commun.* **2016**, *7*, 10484.
(57) Maksimov, A. A.; Bacher, G.; McDonald, A.; Kulakovskii, V. D.; Forchel, A.; Becker, C. R.; Landwehr, G.; Molenkamp, L. W. Magnetic Polarons in a Single Diluted Magnetic Semiconductor Quantum Dot. *Phys. Rev. B: Condens. Matter Mater. Phys.* **2000**, *62*, R7767−R7770.
(58) Bacher, G.; Schömig, H.; Scheibner, M.; Forchel, A.; Maksimov, A. A.; Chernenko, A. V.; Dorozhkin, P. S.; Kulakovskii, V. D.; Kennedy, T.; Reinecke, T. L. Spin−Spin Interaction in Magnetic Semiconductor Quantum Dots. *Phys. E* **2005**, *26*, 37−44.
(59) Kłopotowski, Ł.; Cywiński, Ł.; Wojnar, P.; Voliotis, V.; Fronc, K.; Kazimierczuk, T.; Golnik, A.; Ravaro, M.; Grousson, R.; Karczewski, G.; et al. Magnetic Polaron Formation and Exciton Spin Relaxation in Single $Cd_{1-x}Mn_xTe$ Quantum Dots. *Phys. Rev. B: Condens. Matter Mater. Phys.* **2011**, *83*, 081306.
(60) Kłopotowski, L.; Cywiński, L.; Szymura, M.; Voliotis, V.; Grousson, R.; Wojnar, P.; Fronc, K.; Kazimierczuk, T.; Golnik, A.; Karczewski, G.; et al. Influence of Exciton Spin Relaxation on the Photoluminescence Spectra of Semimagnetic Quantum Dots. *Phys. Rev. B: Condens. Matter Mater. Phys.* **2013**, *87*, 1−12.
(61) Dorozhkin, P. S.; Chernenko, A. V.; Kulakovskii, V. D.; Brichkin, A. S.; Maksimov, A. A.; Schoemig, H.; Bacher, G.; Forchel, A.; Lee, S.; Dobrowolska, M.; et al. Longitudinal and Transverse Fluctuations of Magnetization of the Excitonic Magnetic Polaron in a Semimagnetic Single Quantum Dot. *Phys. Rev. B: Condens. Matter Mater. Phys.* **2003**, *68*, 195313.
(62) Dorozhkin, P. S.; Kulakovskii, V. D.; Chernenko, A. V.; Brichkin, A. S.; Ivanov, S. V.; Toropov, A. A. Controlling Magnetic Moment and Its Fluctuations in Individual Semimagnetic Quantum Dots with Different Exchange Interactions. *Appl. Phys. Lett.* **2005**, *86*, 062507.
(63) Bacher, G.; Maksimov, A. A.; Schömig, H.; Kulakovskii, V. D.; Welsch, M. K.; Forchel, A.; Dorozhkin, P. S.; Chernenko, A. V.; Lee, S.; Dobrowolska, M.; et al. Monitoring Statistical Magnetic Fluctuations on the Nanometer Scale. *Phys. Rev. Lett.* **2002**, *89*, 1272011−1272014.
(64) Mahler, B.; Spinicelli, P.; Buil, S.; Quelin, X.; Hermier, J.-P.; Dubertret, B. Toward Non-Blinking Quantum Dots: The Effect of Thick Shell. In *Colloidal Quantum Dots for Biomedical Applications IV*; Osinski, M., Jovin, T. M., Yamamoto, K., Eds.; International Society for Optics and Photonics: Bellingham WA, 2009; Vol. *7189*, p 718903.
(65) Empedocles, S. A.; Bawendi, M. G. Influence of Spectral Diffusion on the Line Shapes of Single CdSe Nanocrystallite Quantum Dots. *J. Phys. Chem. B* **1999**, *103*, 1826−1830.
(66) Empedocles, S. A.; Norris, D. J.; Bawendi, M. G. Photoluminescence Spectroscopy of Single CdSe Nanocrystallite Quantum Dots. *Phys. Rev. Lett.* **1996**, *77*, 3873−3876.
(67) Fernée, M. J.; Littleton, B. N.; Cooper, S.; Rubinsztein-Dunlop, H.; Gómez, D. E.; Mulvaney, P. Acoustic Phonon Contributions to the Emission Spectrum of Single CdSe Nanocrystals. *J. Phys. Chem. C* **2008**, *112*, 1878−1884.
(68) Varshni, Y. P. Temperature Dependence of the Energy Gap in Semiconductors. *Physica* **1967**, *34*, 149−154.
(69) Madelung, O. *Semiconductors: Data Handbook*, 3rd ed.; Springer: Berlin, 2003.
(70) Furdyna, J. K.; Kossut, K. Dilute Magnetic Semiconductors. In *Semiconductors and Semimetals*; Furdyna, J. K., Kossut, J., Ed.; Academic Press, Inc.: New York, 1988; Vol. *25*.
(71) O'Donnell, K. P.; Chen, X. Temperature Dependence of Semiconductor Band Gaps. *Appl. Phys. Lett.* **1991**, *58*, 2924−2926.
(72) Hernández-Calderón, I. Optical Properties and Electronic Structure of Wide Band Gap II-VI Semiconductors. In *II−VI Semiconductor Materials and Their Applications*; Tamargo, M. C., Ed.; Taylor and Francis: New York, 2002; pp 113−170.
(73) Scott, R.; Prudnikau, A. V.; Antanovich, A.; Christodoulou, S.; Riedl, T.; Bertrand, G. H. V.; Owschimikow, N.; Lindner, J. K. N.; Hens, Z.; Moreels, I.; et al. A Comparative Study Demonstrates Strong Size Tunability of Carrier−Phonon Coupling in CdSe-Based 2D and 0D Nanocrystals. *Nanoscale* **2019**, *11*, 3958−3967.
(74) Yakovlev, D. R.; Ossau, W. Magnetic Polarons. In *Introduction to the Physics of Diluted Magnetic Semiconductors*, Springer Series in Materials Science; Gaj, J. A., Kossut, J., Eds.; Springer: Berlin, Heidelberg, 2010; pp 221−262.
(75) Heiman, D.; Shapira, Y.; Foner, S.; Khazai, B.; Kershaw, R.; Dwight, K.; Wold, A. Exchange Energy, Magnetization, and Raman Scattering of (Cd,Mn)Se. *Phys. Rev. B: Condens. Matter Mater. Phys.* **1984**, *29*, 5634−5640.
(76) Rudin, S.; Reinecke, T. L. Temperature-Dependent Exciton Linewidths in Semiconductor Quantum Wells. *Phys. Rev. B: Condens. Matter Mater. Phys.* **1990**, *41*, 3017−3027.
(77) Al Salman, A.; Tortschanoff, A.; Mohamed, M. B.; Tonti, D.; van Mourik, F.; Chergui, M. Temperature Effects on the Spectral Properties of Colloidal CdSe Nanodots, Nanorods, and Tetrapods. *Appl. Phys. Lett.* **2007**, *90*, 093104.
(78) Landau, L.; Lifshitz, E. M. *Statistical Physics*; Pergamon: New York, 1983.

https://dx.doi.org/10.1021/acs.nanolett.9b05136
Nano Lett. 2020, 20, 1896−1906

(79) Hundt, A.; Puls, J.; Henneberger, F. Spin Properties of Self-Organized Diluted Magnetic $Cd_{1-x}Mn_xSe$ Quantum Dots. *Phys. Rev. B: Condens. Matter Mater. Phys.* **2004**, *69*, 121309.
(80) Henneberger, F.; Puls, J. Diluted Magnetic Quantum Dots. In *Introduction to the Physics of Diluted Magnetic Semiconductors*; Kossut, K., Gaj, J. A., Eds.; Springer: Heidelberg, 2010.
(81) Johnston-Halperin, E.; Awschalom, D. D.; Crooker, S. A.; Efros, A. L.; Rosen, M.; Peng, X.; Alivisatos, A. P. Spin Spectroscopy of Dark Excitons in CdSe Quantum Dots to 60 T. *Phys. Rev. B: Condens. Matter Mater. Phys.* **2001**, *63*, 205309.
(82) Furis, M.; Hollingsworth, J. A.; Klimov, V. I.; Crooker, S. A. Time- and Polarization-Resolved Optical Spectroscopy of Colloidal CdSe Nanocrystal Quantum Dots in High Magnetic Fields. *J. Phys. Chem. B* **2005**, *109*, 15332−15338.
(83) Efros, A.; Rosen, M.; Kuno, M.; Nirmal, M.; Norris, D.; Bawendi, M. Band-Edge Exciton in Quantum Dots of Semiconductors with a Degenerate Valence Band: Dark and Bright Exciton States. *Phys. Rev. B: Condens. Matter Mater. Phys.* **1996**, *54*, 4843−4856.

https://dx.doi.org/10.1021/acs.nanolett.9b05136
Nano Lett. 2020, 20, 1896−1906